Proceedings ASME International Mechanical Engineering Congress and Exhibition, pp. 227-34., Anaheim, CA, 1998.

STABILITY AND PERFORMANCE OF HAPTIC DISPLAYS: THEORY AND EXPERIMENTS

Richard J. Adams * **Manuel R. Moreyra** † **Blake Hannaford** *

* **Department of Electrical Engineering**
University of Washington, Box 352500
Seattle, WA 98195-2500

† **Haptic Technologies Inc.**
4729 40th Avenue NE
Seattle, WA 98105

ABSTRACT

In haptic simulation, a human operator kinesthetically explores a virtual environment. To achieve a virtual sense of touch, the human interacts with an active mechanical device, called a haptic display. This paper presents an approach to guarantee that this physical man-machine interface remains stable, while maximizing performance. The key element in ensuring stability is the virtual coupling network, an artificial link between the haptic display and the virtual environment. Considerations of structural flexibility in the haptic device are included in the derivation of design criteria for such networks. Solutions for both the impedance and admittance models of haptic interaction are included. Numerical and experimental results for a two degree-of-freedom haptic display demonstrate the effectiveness of the proposed approach in achieving performance and stability in haptic simulation.

I. INTRODUCTION

The word *haptic* refers to something that is associated with the sense of touch. A haptic simulation is a combination of elements required to provide a human with an artificial sense of kinesthetic presence in a virtual world. These include, as a minimum, a human operator, a haptic display, and a computer model of the virtual environment. The human operator makes physical contact with the haptic display. A haptic display can take on many forms, but is often some type of robotic manipulator with the ability to exert forces on a human. The virtual environment can represent a physically-motivated or completely contrived world. Applications of haptic simulation include surgical training, physical rehabilitation, computer-aided design, and entertainment.

Stability is critical in haptic simulation. Unlike conventional robotic manipulators which operate in controlled spaces, haptic devices inherently function in close proximity to humans. If a haptic display is powerful enough, an unpredicted instability in a haptic simulation can inflict bodily harm on the operator. Stability depends on all three elements of a haptic simulation. Unfortunately, two of these, the human operator and the virtual environment, can be highly unpredictable. Since classical control techniques are not well adapted to this problem, alternative approaches to guaranteeing the stability of a haptic simulation must be explored.

The field of bilateral teleoperation shares with haptic simulation the need to provide force-feedback cues to a human operator interacting with an unstructured and changing environment. A number of researchers have investigated the use of two-port models to characterize stability and performance in teleoperation. Hannaford introduced a framework for the design of teleoperators based on the two-port hybrid matrix [1]. Anderson and Spong used two-port network theory to guarantee stability for bilateral teleoperation with time delay [2]. In [3], Colgate presented criteria for coupled stability in bilateral systems and introduced an impedance shaping approach to bilateral control.

The use of an artificial coupling between the haptic display and the virtual environment was first proposed by Colgate et. al. [4]. This coupling ensures that the haptic simulation remains stable regardless of the complexity of the virtual environment or of the level of human grasp interaction. Zilles and Salisbury [5] suggested a similar "god-object" approach which couples a haptic device to a virtual environment through a virtual spring-damper. Adams and Hannaford [6] put the problem of stable haptic simulation into a two-port framework and extended the concept of a virtual coupling to include admittance type haptic displays. Using a simple benchmark problem, they identified a duality between the impedance and admittance models of haptic interaction which provides insights into stability and performance tradeoffs for haptic interface design.

This paper presents criteria for the design of virtual coupling networks which guarantee stable haptic interaction, assuming that the human operator and virtual environment are both passive. When such a coupling is found, a passive virtual environment, no matter how complex, can no longer destabilize a haptic simulation. The virtual coupling network thus has the effect of separating haptic display and control design from the problem of virtual environment construction. In the following, the virtual coupling design conditions of [6] are extended to include structural flexibility in the haptic device. Both impedance and admittance type haptic displays are considered. A detailed numerical example demonstrates the design approach. Experimental results on a two degree-of-freedom haptic device show the usefulness of the proposed method.

II. PRELIMINARIES

Two-port Models

Two-port models are widely used in circuit analysis to characterize the behavior of a network with two accessible terminal pairs or ports. A two-port network representation is a "black box" which captures

the relationships between currents and voltages. Two-port forms can also be used in the analysis of mechanical systems by substituting velocities for currents (*flows*) and forces for voltages (*efforts*). These models have become prevalent in the study of bilateral teleoperators [1] and more recently in the analysis and design of haptic interfaces [6].

There are several ways of representing the relationships between efforts and flows in a two-port network. In this paper, we will make frequent use of *immittance matrices* which form a mapping between velocities (v_1, $-v_2$) and forces (F_1, F_2). The negative sign on v_2 is necessary to maintain consistency in notation between electrical circuit networks and our mechanical analog. We will refer to a mapping between two vectors, y and u, as an *immittance mapping* if $y^T u = F_1 v_1 + F_2(-v_2)$. In such a case, P is referred to as an immittance matrix. Possible immittance matrices are the impedance matrix, Z, the admittance matrix, Y, the hybrid matrix, H, and the alternate hybrid matrix, G.

Stability Concepts

A two-port network cannot be defined as stable or unstable without specifying how the accessible ports are terminated. The termination at port i may simply be open-circuit ($v_i = 0$) or short-circuit ($F_i = 0$). More generally, terminating immittances are defined as the combination of impedance, ($F_1 = -Z_1 v_1$, $F_2 = Z_2 v_2$), and admittance functions, ($v_1 = -Y_1 F_1$, $v_2 = Y_2 F_2$), which correspond to the chosen form of the two-port matrix.

Definition 1: A continuous (discrete) linear two-port network with given terminal immittances is *stable* if and only if the corresponding characteristic equation has no roots in the right half s - plane (outside the unit circle, z - plane) and only simple roots on the imaginary axis (unit circle).

Often, the terminating immittances are not a priori known. In this case, it can be useful to define the stability of a two-port for a broad class of terminating immittance functions. Specifically, we will be interested in passive terminations.

Definition 2: A linear two-port is *unconditionally stable* if and only if there exists no set of passive terminating one-port immittances for which the system is unstable [7].

The notion of unconditional stability is closely linked to the concept of the passivity of a two-port network. A passive two-port will always be unconditionally stable, but an unconditionally stable network is not necessarily passive. The two notions are equivalent for reciprocal two-ports ($z_{12} = z_{21}$).

III. HAPTIC SIMULATION

A haptic simulation includes a human operator, a haptic device, and a virtual environment. The human operator makes contact with the haptic device through grasp or some other mechanism. This device, typically some form of robotic manipulator, provides the operator with a kinesthetic sense of presence in the virtual environment through selective application of control forces. Fig. 1 shows the components of a haptic simulation. The human operator and haptic device are coupled through force, F_h, and velocity, v_h. The device is equipped with an actuator which generates force F_d and a sensor from which we can derive velocity v_d. The haptic device may also be fitted with a force sensor that provides a signal F_{meas} (not shown). The motion of the device is coupled to an object in the virtual environment. The object experiences force, F_e, and movement, v_e, according to some physically motivated model of a virtual world

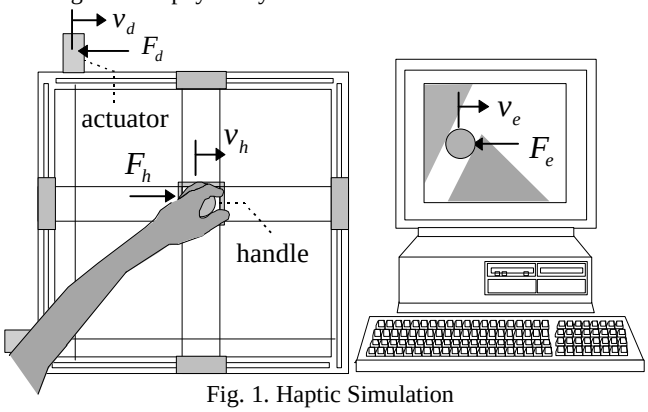

Fig. 1. Haptic Simulation

A haptic device can be implemented in one of two different modes of display: impedance or admittance. An impedance display generates forces in response to measured displacements. Devices which have low-inertia and are highly back-drivable commonly fall into this category. The PHANToM family of force displays is included in this class [8]. Admittance displays generate displacements in response to measured forces. These devices are fitted with force sensors and driven by a servo control loop. They typically have high-inertia and are non back-drivable. The Iowa State/Boeing virtual aircraft control column, based upon a PUMA 560 industrial robot, is an example of an admittance display [9].

A virtual environment is a computer generated model of a physically-motivated scene. It enforces a relationship between velocity, v_e, and force, F_e, at an interaction port in the virtual world. The environmental port can either act as an impedance, $F_e = Z_e v_e$, or as an admittance, $v_e = Y_e F_e$. Impedance methods, also referred to as penalty-based methods, generate forces in response to an object's movement. They have been widely used due to ease of implementation and the ability to represent compliant virtual objects. Environments based on penalty methods often require numerical integration of a stiff set of differential equations, resulting in poor accuracy and stability. Admittance approaches define the motion at the interaction port, v_e, as a function of externally applied forces and internal constraint forces. External forces come from the human operator through the haptic interface. Constraint forces arise from an internal model of the virtual environment.

The haptic display (impedance or admittance) can be coupled to the virtual environment (impedance or admittance) through a virtual coupling network [6]. Fig. 2 shows the entire haptic simulation modeled in network form. Bi-directional arrows indicate that the direction of information flow depends on the choice of haptic architecture. The nominal arrow direction (no parenthesis) shows the flow of information for an impedance display when coupled to an impedance environment. The virtual environment can be switched to admittance type by changing the direction of the arrows for v_e and F_e (in parenthesis). The haptic display can be switched to admittance type by reversing the arrows for v_d and F_d and changing

the appropriate subscripts to those shown in parenthesis. By taking different combinations of display and environment types, four different haptic architectures can be formed. In the special case of impedance display/impedance environment, by far the most common architecture at this writing, the haptic display can be linked to the virtual environment by setting $v_e = v_d$ and $F_d = F_e$. Similarly, in the case of admittance display/admittance environment, a simple coupling is $v_{com} = v_e$, $F_e = F_{meas}$. It was shown in [6] that these, the most commonly used, coupling schemes can lead to an unstable haptic simulation if the design of the virtual environment is not closely linked to the particular haptic display being used.

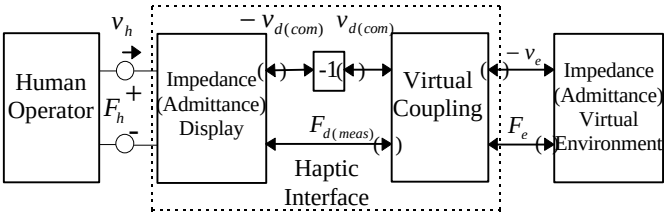

Fig. 2. Network model of Haptic Simulation.

These stability problems motivated the design of virtual coupling networks which guarantee stable haptic simulation. The goal is to form the haptic interface, as defined in Fig. 2, such that the overall haptic simulation will be stable for any passive human operator and passive virtual environment. Referring to Definition 2, this is equivalent to demanding that the haptic interface be unconditionally stable. The benefit of posing the problem in terms of unconditional stability is that the haptic device control problem becomes decoupled from the synthesis of virtual environments. Haptic enabled software can then be developed which stably interfaces to a wide range of haptic devices. For example, the same computer-aided design package could be used with a commercially available PHANToM device, a haptic mouse, or even a PUMA-based device. In each case, stability would be ensured.

To achieve the desired decoupling, the haptic interface must be unconditionally stable, the human operator must be passive, and the virtual environment must be passive. While it is reasonable to treat human interaction with a mechanical device as passive for stability analysis [10], requiring that the virtual environment act as a passive operator can be challenging. It is intuitive that a simulation of a physical world should obey conservation laws of physics, and thus be passive. However, formulating numerical integration routines which achieve strict adherence to these laws is difficult. Fortunately, virtual environments which are "almost" passive work quite well in practice [11]. Virtual coupling networks, designed for unconditional stability, still provide a high level of decoupling between design of control laws and the design of virtual environments.

For linear time-invariant (LTI) two-ports, Llewellyn's stability criteria provide both necessary and sufficient conditions for unconditional stability, regardless of the form of the immittance matrix [7]. In terms of a general two-port immittance matrix P, the criteria are, $\mathrm{Re}(p_{11}) \geq 0$,

$$2\,\mathrm{Re}(p_{11})\mathrm{Re}(p_{22}) \geq |p_{12}p_{21}| + \mathrm{Re}(p_{12}p_{21}), \forall \omega \geq 0 \qquad (1)$$

In [6], Llewellyn's criteria was applied to the analysis and design of virtual coupling networks for a single degree-of-freedom rigid haptic device. It was shown that regardless of whether an impedance or admittance display is used, it is impossible for a haptic interface to stably simulate perfectly free motion, without inertia or friction. When an impedance display is used, it is the open loop device impedance which defines the free-motion response to the human operator. In the case of an admittance display, the minimum impedance is artificially set by the virtual coupling network. A haptic display can never enforce an infinitely rigid constraint. When an admittance display is used, the maximum achieved impedance is defined by the stiffness of its position control loop. In the case of an impedance display, the virtual coupling determines the maximum impedance. Worst case stability for an impedance type haptic display usually occurs when human operator impedance is low (loose grasp or hands-off) and virtual environment impedance is high (rigid constraint). Conversely, worst case stability for an admittance type haptic display normally occurs when human operator impedance is high (rigid grasp) and virtual environment impedance is low (free motion).

There is no consensus on how to quantify the performance of a haptic display. Colgate and Brown [12] suggested using the achievable range of impedance which the haptic interface can stably present to the human operator. This range, or *Z-width*, is delimited by frequency dependent lower and upper bounds, $Z_{\min}$ and $Z_{\max}$. In this paper, we will use the terms *Z*-width and *impedance range* interchangeably.

IV. HAPTIC DISPLAY

We can model a linear single degree-of-freedom haptic device as a chain of lumped masses connected by springs and dampers. The human operator grasps the device at one end of the chain and an actuator applies forces at the other end. Fig. 3 shows the lumped-mass haptic device model.

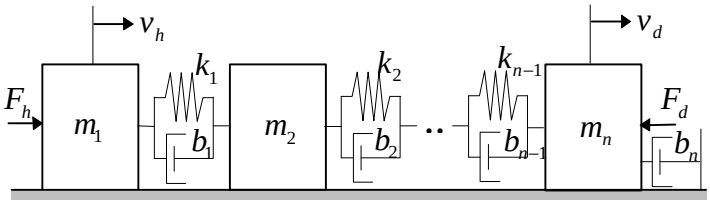

Fig. 3. Haptic Device with Structural Flexibility

To include the effects of digital implementation on stability, the model is discretized using Tustin's method. The Tustin, or bilinear, transform has the important property that the passivity or non-passivity of the continuous-time system is appropriately mapped to the discrete form. Preserving these properties is critical since we are applying passivity-based analysis to determine the stability of our system. Digital implementation requires the introduction of a zero-order hold at the point of actuation, F_d. Eq. (2) defines the two-port admittance properties of an impedance type display.

$$\begin{bmatrix} v_h(z) \\ -v_d(z) \end{bmatrix} = \left(\begin{bmatrix} y_{11}(s) & y_{12}(s) \\ y_{21}(s) & y_{22}(s) \end{bmatrix} \begin{bmatrix} 1 & 0 \\ 0 & 1/s \end{bmatrix} \right)\Bigg|_{s \to \frac{2}{T}\left(\frac{z-1}{z+1}\right)} \begin{bmatrix} 1 & 0 \\ 0 & \left(\frac{z-1}{Tz}\right) \end{bmatrix} \begin{bmatrix} F_h(z) \\ F_d(z) \end{bmatrix}$$

$$= \begin{bmatrix} Y_{11}(z) & Y_{12}(z) \\ Y_{21}(z) & Y_{22}(z) \end{bmatrix} \begin{bmatrix} F_h(z) \\ F_d(z) \end{bmatrix} \qquad (2)$$

To achieve unconditional stability for the combined haptic interface network, we must introduce a virtual coupling which links the haptic display to a virtual environment. In general, the virtual coupling network can have arbitrary structure. For design purposes, it is convenient to consider a simple two port network consisting of a single shunt element. A physically motivated example of such a virtual coupling is a spring-damper with stiffness, k_c, and damping, b_c. This virtual coupling enforces the equations,

$$F_e(s) = F_d(s), \quad F_e(s) = \left(b_c + \frac{k_c}{s} \right)\left(v_d(s) - v_e(s) \right) \tag{3}$$

The discretization of the virtual coupling impedance function can be performed using a rectangular integration approximation,

$$Z_{c_I}(z) = b_c + k_c\left(\frac{Tz}{z-1} \right) \tag{4}$$

The actual implementation of the virtual coupling network depends on the impedance or admittance causality of the virtual environment. When the impedance display is coupled to a impedance (penalty-type) environment, the virtual coupling network is implemented in hybrid form.

$$\begin{bmatrix} F_d(z) \\ -v_e(z) \end{bmatrix} = \begin{bmatrix} 0 & 1 \\ -1 & \dfrac{1}{Z_{c_I}(z)} \end{bmatrix} \begin{bmatrix} v_d(z) \\ F_e(z) \end{bmatrix} \tag{5}$$

For an admittance (constraint-type) environment, the virtual coupling is implemented in impedance form.

$$\begin{bmatrix} F_d(z) \\ F_e(z) \end{bmatrix} = \begin{bmatrix} Z_{c_I}(z) & Z_{c_I}(z) \\ Z_{c_I}(z) & Z_{c_I}(z) \end{bmatrix} \begin{bmatrix} v_d(z) \\ -v_e(z) \end{bmatrix} \tag{6}$$

Returning to analysis, by linking the virtual coupling to the haptic display (2), we form the combined haptic interface admittance mapping,

$$\begin{bmatrix} v_h(z) \\ -v_e(z) \end{bmatrix} = \begin{bmatrix} Y_{11}(z) & Y_{12}(z) \\ Y_{21}(z) & Y_{22}(z) + \dfrac{1}{Z_{c_I}(z)} \end{bmatrix} \begin{bmatrix} F_h(z) \\ F_e(z) \end{bmatrix} \tag{7}$$

Eq. (7) represents the behavior of the haptic interface network, irrespective of whether an impedance or admittance type virtual environment is used. A design for $Z_{c_I}(z)$ which makes (7) unconditionally stable will work equally well for both implementations, (5) and (6), provided that the virtual environment is passive in each case. Note that only the lower-right term in the admittance matrix changes between (2) and (7) with the addition of the virtual coupling. We can directly apply (1) to get necessary and sufficient conditions for unconditional stability,

$$\begin{aligned} &\mathrm{Re}\left(Y_{11}(z)\right) \geq 0, \quad 2\,\mathrm{Re}\left(Y_{11}(z)\right)\mathrm{Re}\left(Y_{22}(z) + 1/Z_{c_I}(z)\right) \\ &\quad \geq \left|Y_{12}(z)Y_{21}(z)\right| + \mathrm{Re}\left(Y_{12}(z)Y_{21}(z)\right) \end{aligned} \tag{8}$$

Rearranging (8) gives us the design equation for the virtual coupling,

$$\mathrm{Re}\left(1/Z_{c_I}(z)\right) \geq \frac{\left|Y_{12}(z)Y_{21}(z)\right| + \mathrm{Re}\left(Y_{12}(z)Y_{21}(z)\right)}{2\,\mathrm{Re}\left(Y_{11}(z)\right)} - \mathrm{Re}\left(Y_{22}(z)\right) \tag{9}$$

We can plot the right-hand side of (9) versus frequency to form a lower bound for $\mathrm{Re}\left(1/Z_{c_I}(z)\right)$. A function $Z_{c_I}(z)$ must then be found which satisfies this bound for all frequencies. By choosing parameters which minimize the additional compliance introduced by the virtual coupling, performance is maximized. For the simple coupling function considered here, (4), it is straightforward to iteratively choose gains and plot $\mathrm{Re}\left(1/Z_{c_I}(z)\right)$ versus the lower bound until the maximum k_c and accompanying b_c are found which satisfy (9).

The performance of the haptic interface network can be quantified in terms of upper and lower bounds on the impedance range. Using (7) and setting $F_e(z) = Z_e(z)v_e(z)$, we can define the resulting one-port admittance function, $Y_p(z)$. This is the admittance presented to the human operator.

$$Y_p(z) = \frac{v_h(z)}{F_h(z)} = Y_{11}(z) - \frac{Y_{12}(z)Y_{21}(z)Z_e(z)}{1 + \left(Y_{22}(z) + 1/Z_{c_I}(z)\right)Z_e(z)} \tag{10}$$

The minimum impedance that the display can present to the human operator is formed by short-circuiting the virtual environment ($Z_e \to 0$),

$$Z_{\min}(z) = \left.\frac{1}{Y_p(z)}\right|_{Z_e(z)\to 0} = \frac{1}{Y_{11}(z)} \tag{11}$$

This function is simply the open loop impedance of the mechanical device. The maximum realizable impedance is found by making the virtual environment port open-circuit ($Z_e \to \infty$),

$$Z_{\max}(z) = \left.\frac{1}{Y_p(z)}\right|_{Z_e(z)\to\infty} = \frac{Y_{22}(z) + 1/Z_{c_I}(z)}{Y_{11}(z)\left(Y_{22}(z) + 1/Z_{c_I}(z)\right) - Y_{12}(z)Y_{21}(z)} \tag{12}$$

The magnitude of this function, and thus performance, is maximized by choosing the greatest values of k_c and b_c for which (9) is satisfied.

Admittance Type Haptic Display

In the admittance model of haptic interaction, the haptic display generates displacements in response to measured forces. We can form an admittance display by adding a displacement control loop and measuring force at the point of device-human contact. The displacement control law can be written as,

$$F_d(z) = K_d(z)\left(v_d(z) - v_{com}(z)\right) \tag{13}$$

where v_{com} is the commanded velocity. The measured force, F_{meas}, often comes from a strain gage mounted on a flexible element, and thus is a function of both the force applied by/to the human, F_h, and the internal state of the device's flexible modes. By applying (13) to (2) and assuming we have a model of force gage dynamics, we can form the alternate hybrid mapping for the admittance display,

$$\begin{bmatrix} v_h(z) \\ F_{meas}(z) \end{bmatrix} = \begin{bmatrix} G_{11}(z) & G_{12}(z) \\ G_{21}(z) & G_{22}(z) \end{bmatrix} \begin{bmatrix} F_h(z) \\ -v_{com}(z) \end{bmatrix} \tag{14}$$

We would like to design a virtual coupling network to guarantee that the admittance display will remain stable when connected to any passive human operator and virtual environment. In general, this coupling may be any two port which creates an unconditionally stable haptic interface network. Restricting the structure of the virtual

coupling network greatly simplifies the development of an explicit design procedure. In the impedance display case, a simple shunt network was used. By duality [6], we can infer that an appropriate virtual coupling for the admittance case will take the form of a simple series network. This coupling provides a minimum driving point impedance at the virtual environment port (v_e , F_e) according to the equations,

$$v_{com}(z) = v_e(z), \quad v_e(z) = \frac{1}{Z_{c_A}(z)}\left(F_{meas}(z) - F_e(z)\right) \tag{15}$$

For the impedance display, the coupling took to form of a spring plus damper connected in parallel. The mechanical dual of this system is a damper plus mass connected in series. The admittance function of the resulting system is

$$Y_{c_A}(z) = \left(\frac{1}{b_c} + \frac{1}{m_c s}\right)\Bigg|_{s \to \left(\frac{z-1}{Tz}\right)} \tag{16}$$

with $Z_{c_A}(z) = 1/Y_{c_A}(z)$.

Again, the actual implementation of the virtual coupling network depends on the causality of the virtual environment. When the admittance display is coupled to an impedance (penalty-type) environment, the virtual coupling network is implemented in admittance form.

$$\begin{bmatrix} v_{com}(z) \\ -v_e(z) \end{bmatrix} = \begin{bmatrix} \frac{1}{Z_{c_A}(z)} & -\frac{1}{Z_{c_A}(z)} \\ -\frac{1}{Z_{c_A}(z)} & \frac{1}{Z_{c_A}(z)} \end{bmatrix} \begin{bmatrix} F_{meas}(z) \\ F_e(z) \end{bmatrix} \tag{17}$$

For an admittance (constraint-type) environment, the virtual coupling is implemented in alternate hybrid form.

$$\begin{bmatrix} v_{com}(z) \\ F_e(z) \end{bmatrix} = \begin{bmatrix} 0 & -1 \\ 1 & Z_{c_A}(z) \end{bmatrix} \begin{bmatrix} F_{meas}(z) \\ -v_e(z) \end{bmatrix} \tag{18}$$

Combining the virtual coupling with the admittance display, (14), we get the alternate hybrid matrix for the haptic interface,

$$\begin{bmatrix} v_h(z) \\ F_e(z) \end{bmatrix} = \begin{bmatrix} G_{11}(z) & G_{12}(z) \\ G_{21}(z) & G_{22}(z) + Z_{c_A}(z) \end{bmatrix} \begin{bmatrix} F_h(z) \\ -v_e(z) \end{bmatrix} \tag{19}$$

which represents the behavior of the haptic interface network, regardless of whether (17) or (18) is used to implement the virtual coupling. The addition of the virtual coupling changes only the lower-right terms between (14) and (19). By applying (1), we get the following necessary and sufficient conditions for unconditional stability,

$$\begin{aligned} &\mathrm{Re}\left(G_{11}(z)\right) \geq 0, \quad 2\,\mathrm{Re}\left(G_{11}(z)\right)\mathrm{Re}\left(G_{22}(z) + Z_{c_A}(z)\right) \\ &\quad \geq \left|G_{12}(z)G_{21}(z)\right| + \mathrm{Re}\left(G_{12}(z)G_{21}(z)\right) \end{aligned} \tag{20}$$

Rearranging (20) gives us the virtual coupling design equation for an admittance display,

$$\mathrm{Re}\left(Z_{c_A}(z)\right) \geq \frac{\left|G_{12}(z)G_{21}(z)\right| + \mathrm{Re}\left(G_{12}(z)G_{21}(z)\right)}{2\,\mathrm{Re}\left(G_{11}(z)\right)} - \mathrm{Re}\left(G_{22}(z)\right) \tag{21}$$

By plotting the right-hand side of (21) versus frequency, we can form a lower bound for $\mathrm{Re}\left(Z_{c_A}(z)\right)$. If we choose the coupling according to (16), our design procedure is simply to choose m_c and b_c such that $\mathrm{Re}\left(Z_{c_A}(z)\right)$ minimally exceeds this bound. The resulting coupling will theoretically give the best possible free motion performance for the admittance display.

Once again, performance is measured in term of upper and lower bounds on the impedance range. Using (19) and setting $v_e(z) = Y_e(z)F_e(z)$, we can define the one-port admittance function, $Y_p(z)$,

$$Y_p(z) = \frac{v_h(z)}{F_h(z)} = G_{11}(z) - \frac{G_{12}(z)G_{21}(z)Y_e(z)}{1 + \left(G_{22}(z) + Z_{c_A}(z)\right)Y_e(z)} \tag{22}$$

The minimum realizable impedance is,

$$Z_{\min}(z) = \frac{1}{Y_p(z)}\Bigg|_{Y_e(z)\to\infty} = \frac{G_{22}(z) + Z_{c_A}(z)}{G_{11}(z)\left(G_{22}(z) + Z_{c_A}(z)\right) - G_{12}(z)G_{21}(z)} \tag{23}$$

This function is minimized by choosing the smallest allowable values for m_c and b_c. The maximum impedance is,

$$Z_{\max}(z) = \frac{1}{Y_p(z)}\Bigg|_{Y_e(z)\to 0} = \frac{1}{G_{11}(z)} \tag{24}$$

The magnitude of this function is determined by the inner loop displacement control law $K_d(z)$. If very rigid virtual constraints are required, the inner loop gains must be high.

V. THE HIGH-BANDWIDTH FORCE-DISPLAY

The High-Bandwidth Force Display (HBFD) is a two degree-of-freedom, planar, haptic display with cartesian kinematics [13]. A large workspace of $300\,mm \times 400\,mm$ and a high force output of 100 N (peak to 400 N), make the device well suited for full arm manipulation in virtual environments. A 266 MHz Pentium II PC provides computational power for the HBFD with interrupt level software running at 1000 Hz ($T = 1.0\,ms$). In both the *x*- and *y*- axis, brushless motors drive a pair of cable transmissions through a rotating torque shaft. Each pair of cable transmissions is coupled by a pair of linear motion shafts. Sliding in planar motion on the linear shafts is a stage, with a handle mounted on top. A load cell between the stage and the handle measures interaction forces between the device and the human operator. Fig. 1 shows the HBFD. The primary sources of compliance in the device are the rotating torque shafts and associated shaft couplers, the cable transmissions, the linear motion shafts, and the load cell. Of these, the most significant are the linear motion shafts. Fig. 4 shows a one degree-of-freedom model of HBFD flexibility [13].

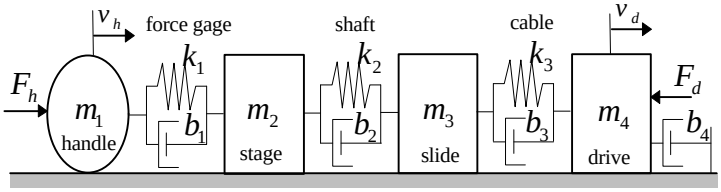

Fig. 4. Lumped-Mass Model of HBFD Flexibility.

This form leads to a dynamical model with three flexible modes and one rigid body mode.

$$\begin{bmatrix} m_1 & 0 & 0 & 0 \\ 0 & m_2 & 0 & 0 \\ 0 & 0 & m_3 & 0 \\ 0 & 0 & 0 & m_4 \end{bmatrix}\begin{bmatrix} \ddot{x}_1 \\ \ddot{x}_2 \\ \ddot{x}_3 \\ \ddot{x}_4 \end{bmatrix}+\begin{bmatrix} b_1 & -b_1 & 0 & 0 \\ -b_1 & b_1+b_2 & -b_2 & 0 \\ 0 & -b_2 & b_2+b_3 & -b_3 \\ 0 & 0 & -b_3 & b_3+b_4 \end{bmatrix}\begin{bmatrix} \dot{x}_1 \\ \dot{x}_2 \\ \dot{x}_3 \\ \dot{x}_4 \end{bmatrix}+$$
$$\begin{bmatrix} k_1 & -k_1 & 0 & 0 \\ -k_1 & k_1+k_2 & -k_2 & 0 \\ 0 & -k_2 & k_2+k_3 & -k_3 \\ 0 & 0 & -k_3 & k_3 \end{bmatrix}\begin{bmatrix} x_1 \\ x_2 \\ x_3 \\ x_4 \end{bmatrix}=\begin{bmatrix} F_h & 0 \\ 0 & 0 \\ 0 & 0 \\ 0 & -F_d \end{bmatrix} \quad (25)$$

The outputs of interest are handle velocity, v_h (m/s), device velocity, v_d (m/s), and measured force , F_{meas} (N).

$$\begin{bmatrix} v_h \\ -v_d \end{bmatrix}=\begin{bmatrix} 1 & 0 & 0 & 0 \\ 0 & 0 & 0 & -1 \end{bmatrix}\begin{bmatrix} \dot{x}_1 & \dot{x}_2 & \dot{x}_3 & \dot{x}_4 \end{bmatrix}^T \quad (26)$$

$$F_{meas}=\begin{bmatrix} -k_3 & k_3 & 0 & 0 \end{bmatrix}\begin{bmatrix} x_1 & x_2 & x_3 & x_4 \end{bmatrix}^T + \begin{bmatrix} -b_3 & b_3 & 0 & 0 \end{bmatrix}\begin{bmatrix} \dot{x}_1 & \dot{x}_2 & \dot{x}_3 & \dot{x}_4 \end{bmatrix}^T \quad (27)$$

Device velocity is derived by a first-order difference approximation using incremental encoder position measurements. The encoders are located on the motors and provide 0.015 mm spatial resolution. Force is measured by a strain gage bridge built into the handle which provides a maximum 0.05 N resolution. Handle velocity is not actually measured, but its theoretical value is required for two-port stability analysis.

A nominal set of masses which adequately characterize the behavior of the HBFD is $m_1 = 0.2\,kg$, $m_2 = 2.3\,kg$, $m_3 = 2.0\,kg$, and $m_4 = 0.5\,kg$. The flexibility of the manipulator varies with the location of the stage. The worst-case configuration, where resonant frequencies are the lowest, occurs when the handle is centered between the two stops. The corresponding stiffness values are $k_1 = 130\,kN/m$, $k_2 = 84\,kN/m$, and $k_3 = 874\,kN/m$. Accurately determining damping parameters is difficult, since both viscous and Coulomb friction are present. A damping ratio of *0.1* is assumed in the flexible elements. The resulting parameters are,

$$b_i = 0.1 \times 2\sqrt{k_i\, m_i m_{i+1}/\left(m_i + m_{i+1}\right)},\ i = 1,2,3 \quad (28)$$

The chosen value for rigid body damping, $b_4 = 5.0\ N/\left(m/s\right)$, while only an approximation, does a reasonable job of representing the behavior of the device.

VI. ANALYSIS AND EXPERIMENTAL RESULTS

Because it is both back-drivable and equipped with a force sensor, the HBFD can be configured to operate as either an impedance or an admittance type haptic display. The friction and inertia of the device fall between the low typical values for impedance displays such as a PHANToM, and the high typical values for admittance displays such as PUMA based implementations. In the following, virtual coupling networks are designed for each configuration. These designs are then implemented on the HBFD to form the haptic interface. The cartesian structure of the HBFD allows each design, based upon the single-axis linear model described above, to be applied independently in each axis of motion (*x* and *y*).

Each virtual coupling network is tested with both impedance and admittance type virtual environments, so that all four haptic architectures are explored. For this study, the virtual environment consists of fixed, two-dimensional objects of different shapes and orientations. There is a single moving object, O_e, whose motion and reaction forces in the *x*- and *y*-axis are linked to the haptic display through the virtual coupling network. This object is simulated as a rigid sphere (circle) of radius *r* and mass m_e.

The impedance environment uses a classic penalty approach to calculate reaction forces based on Hooke's law,

$$F_e = k_{obj}\Delta x \quad (29)$$

where k_{obj} is the stiffness of a virtual object and Δx is the amount of interpenetration. The object O_e is considered massless. Rigid collisions are simulated by setting the stiffness parameter to be very large, $k_{obj} = 500\,kN/m$. For free motion, we simply set $F_e = 0$. The position and velocity of O_e are determined by the virtual coupling network.

The admittance environment implementation is greatly simplified by considering a virtual environment made up solely of fixed objects. In this special case, there is no need to calculate the forces required to prevent object interpenetration. To simulate rigid contact, we can simply constrain the position of O_e to lie on the surface of the interpenetrated object, ($v_e = 0$). This approach is highly reminiscent of the "god-object" technique. The reader is referred to [5] for details. To ideally simulate free motion (zero inertia, zero damping), the virtual environment would have to enforce $v_e = \infty F_e$. In practice, we assume a minimal level of inertia for O_e in order to ensure numerically stable integration ($m_e = 0.02\,kg$).

Impedance Display Implementation

By taking the Laplace transform of equations (25) and (26), it is straightforward to create the continuous-time admittance mapping. With a zero-order hold applied at the point of actuation, F_d, Tustin's method is used to get the discrete form, (2). We can now plot the right-hand side of (9) versus frequency to form a theoretical lower bound for $\mathrm{Re}\left(1/Z_{c_1}(z)\right)$. This lower bound is shown in Fig. 5 as a shaded solid line. If we choose $k_{c_1} = 110\,kN/m$ and $b_{c_1} = 100\,Ns/m$ as the spring and damping constants of the virtual coupling, the resulting plot of $\mathrm{Re}\left(1/Z_{c_1 1}(z)\right)$, shown as a dashed line, just barely exceeds the lower bound. Based upon the linear HBFD model described above, these spring and damping values define the virtual coupling which achieves maximum performance while making the combined haptic interface network (7) unconditionally stable.

The next step is to implement the virtual coupling design in software. With the HBFD configured in impedance display mode, the device was coupled to both impedance and admittance type virtual environments using (5) and (6). In both cases, the resulting haptic simulation had oscillatory (unstable) behavior when the human operator interacted with rigid virtual objects.

The virtual coupling parameters were then tuned experimentally to find the maximum values for which the haptic simulation remained stable and oscillation-free. The worst-case scenario for the

impedance display implementation is when the virtual environment simulates a rigid constraint and the human operator releases the handle of the haptic display. Under these conditions, the haptic simulation was stabilized when the virtual coupling gains were reduced to $k_{c_2} = 50 kN/m$ and $b_{c_2} = 100 Ns/m$. These gains define a new virtual coupling, $Z_{c_I 2}(z)$. A plot of $\mathrm{Re}\left(1/Z_{c_I 2}(z)\right)$ versus frequency is shown in Fig. 5 as a solid line.

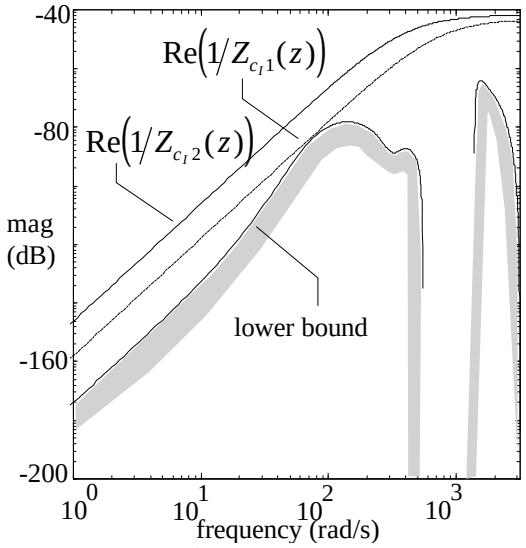

Fig. 5. Stability Results for Impedance Display Implementation.

Two possible explanations for the mismatch between numerical and experimental results are uncertain damping and implementation delay. The lower bound generated by (9) is highly sensitive to the assumed level of damping. The presence of nonlinear friction (e.g. Coulomb friction) can make it difficult to accurately predict performance. In hindsight, if we had assumed a different rigid body damping level, $b_4 = 1.2\ Ns/m$ instead of $5.0\ Ns/m$, the numerical and experimental results would both have yielded $k_c = 50 kN/m$. Implementation delay is another factor which degrades experimental performance. In order to sequentially implement the numerical integration of the virtual coupling and virtual environment equations, a pure delay of *T* seconds must be inserted between them. This is known as explicit integration, the inputs at the *kth* step are a function of outputs delayed by at least one time step. To avoid this delay, an implicit integration technique may be used, but the resulting implementation requires that the virtual coupling and virtual environment equations be combined. Since the virtual environment can be complex and time varying, a general implicit solution is elusive. Brown and Colgate have investigated the explicit/implicit integration problem more thoroughly [11].

Dashed lines in Fig. 6 show the upper and lower bounds on achievable impedance, in *Ns/m*. The plot is calculated using (11) and (12) with the experimentally determined virtual coupling parameters. The shaded region indicates the range of impedance which can be simulated by the impedance display implementation. The upper bound indicates the maximum position stiffness that the human operator may perceive in a rigid virtual object, $k_{\max} = 24.5 kN/m$. The steady-state value of the lower bound corresponds roughly to the minimum damping that the user feels when the virtual environment simulates free motion. This value is the same as the open loop damping of the device, $b_{\min} = 5 Ns/m$.

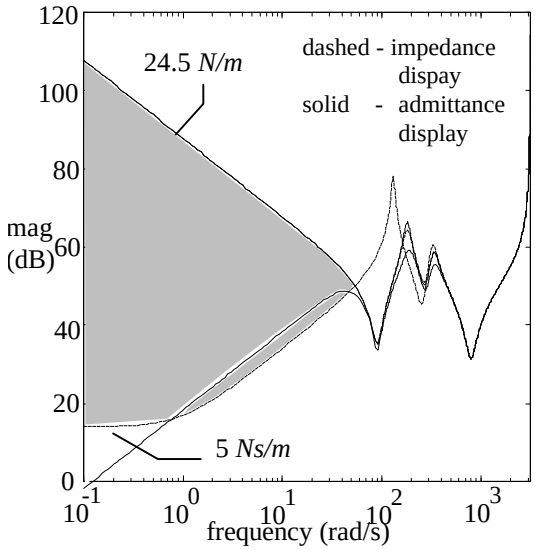

Fig. 6. Impedance Range for Impedance/Admittance Display

Admittance Display Implementation

To create an admittance display from the HBFD, we introduce a proportional-plus-derivative (*PD*) position control loop. Assuming a first-order backwards-difference velocity approximation, the discrete form of the displacement control law in (13) is,

$$K_d(z) = k_p\left(\frac{Tz}{z-1}\right) + k_d \tag{30}$$

By applying (27) and (30) to the discrete-time device admittance mapping (2), we can form the alternate hybrid mapping of the admittance display, (14).

The lower bound defined by the right-hand side of (21) is a function of the *PD* control law parameters. It was shown in [6] that the displacement control law of the admittance display plays an identical role to the virtual coupling of the impedance display in determining the maximum impedance that can be conveyed to the human operator. If we set $k_p = 50 kN/m$ and $k_d = 100 Ns/m$, we can expect that the admittance display will achieve the same upper bound on impedance range as the impedance display implementation.

The unconditional stability bound is shown in Fig. 7 as a shaded solid line. The virtual coupling in this case is defined by the mass and damping terms, m_c and b_c. Based upon the linear model and estimated parameters, the smallest values for which the virtual coupling meets the requirements for unconditional stability are $m_{c_1} = 31 kg$ and $b_{c_1} = 1{,}550 Ns/m$. Fig. 7 shows that the resulting plot of $\mathrm{Re}\left(Z_{c_A 1}(z)\right)$ just exceeds the lower bound.

The virtual coupling design was implemented in software and tested on the HBFD. The device, configured in admittance display mode, was coupled to both impedance and admittance type virtual environments using (17) and (18). The resulting haptic simulation was stable in both cases, even for the worst-case scenario of low virtual environment impedance and high human grasp impedance.

The virtual coupling parameters were reduced to experimentally find the minimum values for which the haptic simulation remains stable and oscillation-free under worst-case conditions. The resulting values are $m_{c_2} = 8 Ns^2/m$ and $b_{c_2} = 400\, Ns/m$. The experimental value is shown in Fig. 7 as a solid line. The primary reason for the difference between numerical and experimental results in this case is likely the limited impedance of the human operator. If $\mathrm{Re}\left(Z_{c_A}(z)\right)$ exceeds the lower bound, unconditional stability is achieved, which implies that the haptic interface will be stable for any passive human impedance, even if it has infinite magnitude and bandwidth. Of course, even with great effort, the human operator will have finite, band-limited impedance. Consequently, the theoretical bound on $\mathrm{Re}\left(Z_{c_A}(z)\right)$ appears to be conservative for an admittance display implementation.

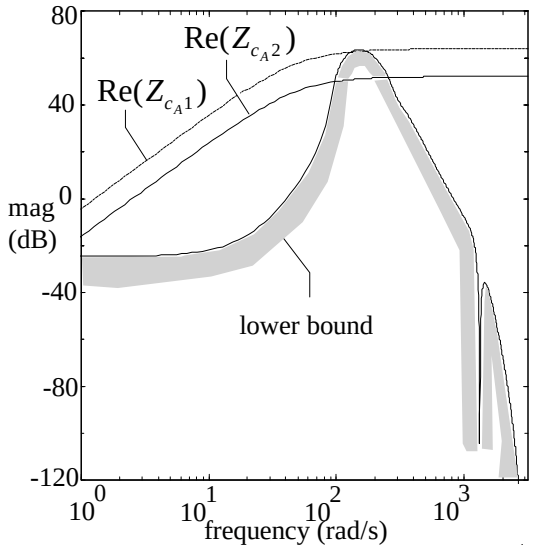

Fig. 7. Stability Results for Admittance Display Implementation.

Solid lines in Fig. 6 show the upper and lower bounds for the impedance range of the admittance display implementation, calculated using (23) and (24) and the experimental virtual coupling parameters. We see that by selecting $K_d(z) = Z_{c_l 2}(z)$, the admittance display has the same upper bound as the impedance display. The bounds on minimum displayable impedance are similar, but not identical. The admittance display achieves very low steady state impedance, while the impedance display exhibits the damping of the open loop device. The admittance display does not do as well in the 1 to 100 *rad/s* range, where the impedance display achieves lower impedance. To the human operator, the admittance display appears to have much lower damping (~ 0 vs. $\sim 5 Ns/m$) but higher inertia than the impedance display ($\sim 8 kg$ vs. $\sim 5 kg$) when simulating free motion.

It may be possible to achieve performance beyond that described above. One potential performance improving step is to go beyond the single shunt and single series two port networks used as virtual couplings in this paper to more general structures. Design criteria for such networks which guarantee unconditional stability do not yet exist. For some applications, the unconditional stability requirement may be too restrictive. The addition of adaptation in the virtual coupling might guarantee stable operation with less conservative performance.

VII. CONCLUSIONS

Stability is a critical consideration in haptic simulation, since there is a risk of physical harm to the human operator. We have used two-port network theory to develop new conditions for the design of virtual coupling networks which guarantee stable haptic simulation when the haptic device includes significant structural flexibility. A detailed numerical example and experimental results have demonstrated the design of virtual coupling networks for a planar haptic display. By considering both impedance and admittance type displays, the procedure is applicable to most existing haptic devices.

VIII. REFERENCES

[1] B. Hannaford, "A Design Framework for Teleoperators with Kinesthetic Feedback," *IEEE Trans. Robotics and Automation*, vol. 5, no. 4, 1989, pp. 426-434.

[2] R.J. Anderson and M.W. Spong, "Asymptotic Stability for Force Reflecting Teleoperators with Time Delay," *Int. Journal of Robotics Research*, vol. 11, no. 2, 1992, pp. 135-49.

[3] J.E. Colgate, "Robust Impedance Shaping Telemanipulation," *IEEE Trans. Robotics and Automation*, vol. 9, no. 4, 1993, pp. 374-384.

[4] J.E. Colgate, et. al., "Implementation of Stiff Virtual Walls in Force-Reflecting Interfaces," *Proc. IEEE Virtual Reality Annual Int. Symposium*, Seattle, WA, 1993, pp. 202-8.

[5] C.B. Zilles and J.K. Salisbury, "A Constraint-based God-object Method for Haptic Display," *Proc. IEEE/RSJ Int. Conf. on Intelligent Robots and Systems*, Pittsburgh, PA, 1995, pp. 146-151.

[6] R.J. Adams and B. Hannaford, "A Two-Port Framework for the Design of Unconditionally Stable Haptic Interfaces," *Proc. IROS*, Anaheim, CA, 1998.

[7] F.B. Llewellyn, "Some Fundamental Properties of Transmission Systems," *Proc. IRE*, vol. 40, 1952, pp. 271-283.

[8] T.H. Massie and J.K. Salisbury, "The Phantom Haptic Interface: A Device for Probing Virtual Objects," *Proceedings of the ASME International Mechanical Engineering Congress and Exhibition*, Chicago, 1994, pp. 295-302.

[9] C.L. Clover, G.R. Luecke, J.J. Troy, and W.A. McNeely, "Dynamic Simulations of Virtual Mechanisms with Haptic Feedback Using Industrial Robotics Equipment," *Proceedings IEEE Int. Conf. Robotics and Automation*, Albuquerque, NM, 1997, pp. 3205-10.

[10] N. Hogan, "Multivariable Mechanics of the Neuromuscular System," *IEEE Eighth Annual Conference of the Engineering in Medicine and Biology Society*, Fort Worth, TX, 1986, pp. 594-598.

[11] J.M. Brown and J.E. Colgate, "Passive Implementation of Multibody Simulations for Haptic Display," *Proceedings of the ASME International Mechanical Engineering Congress and Exhibition*, Dallas, 1997.

[12] J.E. Colgate and J.M. Brown, "Factors Affecting the Z-width of a Haptic Display," *Proceedings IEEE Int. Conf. Robotics and Automation*, Los Alamitos, CA, 1994, pp. 3205-10.

[13] M. R. Moreyra and B. Hannaford, "A Practical Measure of Dynamic Response of Haptic Devices," *Proceedings IEEE Int. Conf. Robotics and Automation*, Leuven, Belgium, 1998, pp. 369-374.